Available online at www.sciencedirect.com
ScienceDirect
Journal of Luminescence 128 (2008) 1211–1216
JOURNAL OF LUMINESCENCE
www.elsevier.com/locate/jlumin

Green and red up-conversion emissions of Er^{3+}–Yb^{3+} Co-doped TiO_2 nanocrystals prepared by sol–gel method

Qingkun Shang[a,b], Hui Yu[b], Xianggui Kong[a,*], Hongdan Wang[b], Xin Wang[a], Yajuan Sun[a], Youlin Zhang[a], Qinghui Zeng[a]

[a]*Key Laboratory of Excited-State Process, Changchun Institute of Optics Fine Mechanics and Physics, Chinese Academy of Sciences, Changchun 130033, PR China*

[b]*Faculty of Chemistry, North-East Normal University, Changchun 130024, PR China*

Received 21 March 2007; received in revised form 23 November 2007; accepted 29 November 2007
Available online 17 December 2007

Abstract

In this paper, green and red up-conversion emissions of Er^{3+}–Yb^{3+} co-doped TiO_2 nanocrystals were reported. The phase structure, particle size and optical properties of Er^{3+}–Yb^{3+} co-doped TiO_2 nanocrystals samples were characterized by using X-ray diffraction (XRD), transmission electron microscopy (TEM), UV–vis–NIR absorption spectra and photoluminescence (PL) spectra. Green and red up-conversion emissions in the range of 520–570 nm ($^2H_{11/2}$, $^4S_{3/2}\rightarrow{}^4I_{15/2}$) and 640–690 nm ($^4F_{9/2}\rightarrow{}^4I_{15/2}$) were observed for the Er^{3+}–Yb^{3+} co-doped TiO_2 nanocrystals. The visible up-conversion mechanism and temperature dependence of up-conversion emission for Er^{3+} in TiO_2 nanocrystals were discussed in detail.
© 2008 Elsevier B.V. All rights reserved.

Keywords: Up-conversion emissions; Er^{3+}–Yb^{3+} co-doped; TiO_2 nanocrystal

1. Introduction

Rare-earth ion doped materials have played an important role in the development of optical communication technology during the past few decades [1–8]. Recently, up-conversion emission in terms of absorption of two or more lower-energy photons followed by emission of a higher-energy photon has attracted much attention due to available low-cost near-infrared laser diodes. Erbium (III) is suitable for the up-conversion of infrared to visible light because of a favorable electronic level scheme with equally spaced, long-lived excited states. Potential applications in optical devices, such as color display, optical data storage, biomedical diagnostics and temperature sensors, have been developed on the basis of up-conversion emission of Er^{3+}–Yb^{3+}-co-doped materials [9,10]. Up to now, several papers have reported the up-conversion properties of Er^{3+} doped in TiO_2 thin films [11], nanocrystallites [12] or glasses [13].

In this work, Er^{3+}–Yb^{3+} co-doped titania nanocrystals were successfully synthesized by the sol–gel process. Green and red emission of Er^{3+} in TiO_2 nanocrystals under the infrared excitation via up-conversion and the energy transfer process from Yb^{3+} were observed.

2. Experimental section

All reagents were analytical grade. $RE(NO_3)\cdot 6H_2O$ (RE = Er and Yb) salt was freshly prepared by the reaction of RE_2O_3 with nitric acid. The concentration of RE in aqueous solution was 0.1 mol/L. Water was distilled and deionized using a Millipore Milli-Q Purification System.

The sol–gel method was used for the preparation of Er^{3+}–Yb^{3+}co-doped TiO_2 nanocrystals. Titanium isopropoxide was used as the precursor for titania sol preparation. 3.4 mL titanium isopropoxide was added to the mixture of 2.0 mL acetic acid and 16.0 mL ethanol. The sol was then stirred for half hour meanwhile 1.0 mL water was added dropwise. Then a certain amount $Er(NO_3)_3$ and

*Corresponding author. Tel.: +86 431 86176313.
E-mail address: xgkong14@ciomp.ac.cn (X. Kong).

0022-2313/$ - see front matter © 2008 Elsevier B.V. All rights reserved.
doi:10.1016/j.jlumin.2007.11.097

$Yb(NO_3)_3$ was added and the sol was stirred for one more hour. The obtained products were dried at 60 °C in vacuum oven for 12 h and then calcined for 4 h at different temperatures 600–800 °C.

The crystal phase of calcined samples was identified by powder X-ray diffraction (XRD). The XRD patterns of the different samples recorded with different temperatures were acquired using a Japan Rigaku D/max-rA X-ray diffractometer system with a monochromatized Cu Kα radiation. ($\lambda = 1.5418$ Å).

Transmission electron microscopy (TEM) observations were completed on a Hitachi H-8100 IV microscope operating at 200 KV. UV–vis–NIR absorption spectra were measured at room temperature with a CARY 500 Scan UV–vis–NIR spectrophotometer.

The emission spectra of Er^{3+}–Yb^{3+} co-doped TiO_2 nanocrystals was measured using a Jobin-Yvon LabRam Raman spectrometer system equipped with 600 and 1800 grooves/mm holographic gratings and a Peltier air-cooled CCD detector. Precise control of sample temperature (±0.1 °C) was achieved by means of a Linkam THMS 600 temperature programmable heating/cooling microscope stage. The THMS stage was used in conjunction with a Linkam LNP cooling system when cooling. VA-I-DC external 980 nm (2 W) semiconductor solid laser was used as the excitation source.

3. Results and discussion

3.1. Structural and morphological investigations

Fig. 1 represents the XRD patterns of TiO_2 nanocrystals before and after Er^{3+} or/and Yb^{3+} ions doping that were calcined at 973 K. It is shown that the rutile phase and the anatase phase are present in the sample without rare-earth ions, where the former dominates. The anatase phase dominates after doping with rare-earth ions.

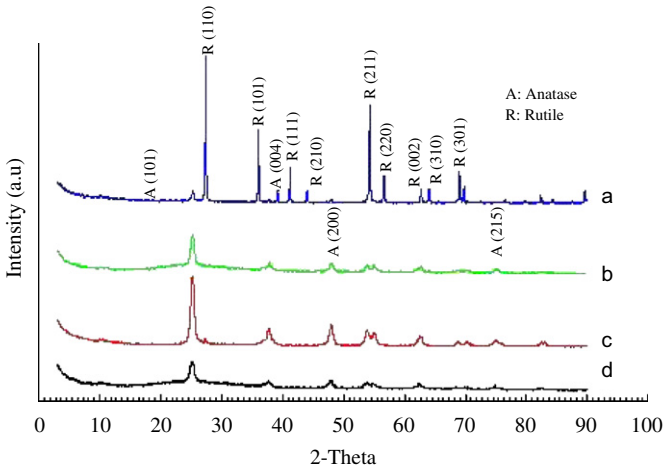

Fig. 1. Powder X-ray diffraction patterns of samples (calcined at 973 K for 4 h) (a) TiO_2 nanocrystals; (b) Yb^{3+} (10 mol%) doped TiO_2 nanocrystals; (c) Er^{3+} (10 mol%) doped TiO_2 nanocrystals; (d) Er^{3+} (10 mol%)–Yb^{3+} (10 mol%) co-doped TiO_2 nanocrystals.

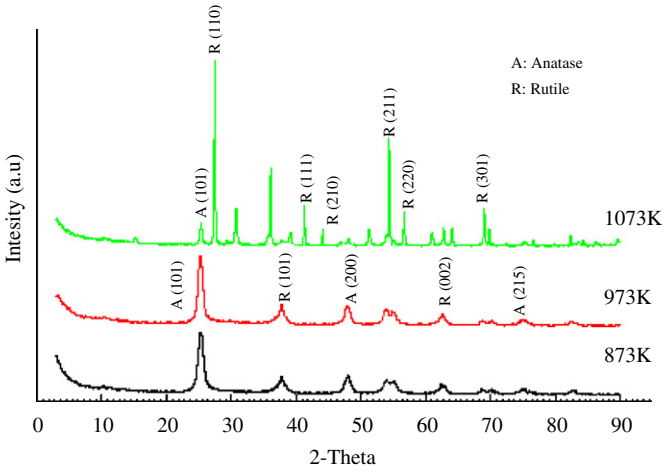

Fig. 2. Powder X-ray diffraction patterns of Er^{3+} (10 mol%)–Yb^{3+} (10 mol%) co-doped TiO_2 sample calcined at different temperatures.

Fig. 2 shows the XRD of Er^{3+}–Yb^{3+} co-doped TiO_2 nanocrystals calcined at different temperatures. It can be seen that the rutile phase dominates when the final temperature is 1073 K while the anatase phase dominates after doping with rare-earth ions below this temperature. Anatase is a metastable phase that can transform into rutile at different temperatures depending on impurities, calcination temperature, crystal size, sample history, etc. [14]. In the present work, rare-earth ions are added as impurities. Calcination temperature is another reason for the phase conversion.

The crystal sizes of the nanoparticles can be calculated using Scherrer's equation

$$D = \frac{K\lambda}{\beta \cos\theta} \quad (1)$$

where $K = 0.9$; D represents the crystallite size (Å); λ is the wavelength of Cu Kα radiation and β is the corrected half width of the diffraction peak.

The average particle sizes of TiO_2 nanocrystals calculated according to Eq. (1) are shown in Table 1. The particle sizes are 102, 22, 21 and 13 nm for sample of TiO_2 nanocrystals without rare-earth doping, and with 10 mol% Er^{3+}, 10 mol% Yb^{3+}, 10 mol% Er^{3+}–10 mol% Yb^{3+} doping, respectively. When the sample is processed at 873, 973 and 1073 K, the average particle sizes are 11, 13 and 67 nm.

Fig. 3 shows TEM image of Er^{3+}–Yb^{3+} co-doped TiO_2 nanocrystals prepared at 973 K. The size of most nanocrystals is found to be less than 20 nm in diameter, which is in accordance with XRD result, i.e. an average diameter of 13 nm.

3.2. Optical properties of Er^{3+}–Yb^{3+} co-doped TiO_2 nanocrystals

The UV–vis–NIR absorption spectra of Er^{3+}–Yb^{3+} co-doped TiO_2 nanocrystals are shown in Fig. 4. The

Table 1
Particle sizes of TiO_2 nanocrystals on different process

Annealing temperature (K)	Particle size of TiO_2 nanocrystals (nm)			
	No RE^{3+}	+10 mol% Er^{3+}	+10 mol% Yb^{3+}	+10 mol% Er^{3+}–10 mol% Yb^{3}
873				11
973	102	22	21	13
1073				67

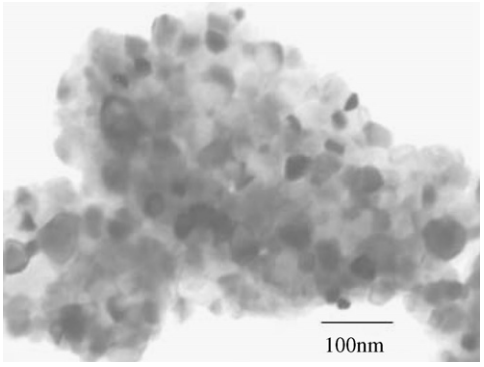

Fig. 3. TEM image of Er^{3+}–Yb^{3+} co-doped TiO_2 nanocrystals calcined at 973 K.

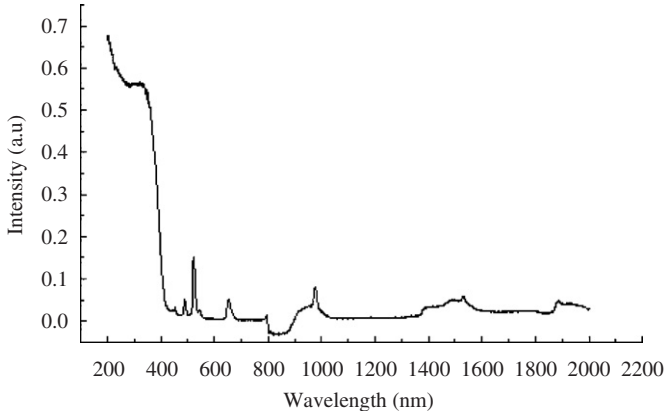

Fig. 4. UV–vis–NIR adsorption spectra of Er^{3+}–Yb^{3+} co-doped TiO_2 nanocrystals powder calcined at 973 K.

absorption peaks at 220 and 300–350 nm are attributed to charge transfer from valence band to conduction band of TiO_2 nanocrystals. Peaks at 489, 522, 654, 795, 976 and 1531 nm are associated with the $^4F_{7/2}\rightarrow{}^4I_{15/2}$, $^2H_{11/2}\rightarrow{}^4I_{15/2}$, $^4F_{9/2}\rightarrow{}^4I_{15/2}$, $^4I_{9/2}\rightarrow{}^4I_{15/2}$ $^4I_{11/2}\rightarrow{}^4I_{15/2}$, $^4I_{13/2}\rightarrow{}^4I_{15/2}$ transitions of Er^{3+} ions, respectively. Peak at 976 nm is associated with $^2F_{5/2}\rightarrow{}^2F_{7/2}$ transition of Yb^{3+} at the same time.

3.3. Up-conversion luminescence properties

Continuous wave excitation with a 980 nm semiconductor laser at room temperature produces up-conversion emission of Er^{3+} (10 mol%)–Yb^{3+} (10 mol%) co-doped TiO_2 nanocrystals in the visible region, as shown in Fig. 5 along with the energy level diagrams of Er^{3+} and Yb^{3+} ions. The green emission in 520–570 nm is assigned to the $(^2H_{11/2},{}^4S_{3/2})\rightarrow{}^4I_{15/2}$ transition and the red emission in 640–690 nm is assigned to the $^4F_{9/2}\rightarrow{}^4I_{15/2}$ transition for the Er^{3+} in TiO_2 nanocrystals. It is obvious that both green and red up-conversion emission intensities are enlarged with Yb^{3+} ion doping with the red emission being stronger than the green one.

Fig. 6 shows the upconverted luminescence spectra in 500–750 nm for three samples of Er^{3+}–Yb^{3+} co-doped TiO_2 nanocrystals prepared at 873, 973 and 1073 K, respectively. It is evident that the up-conversion luminescence intensity increases remarkably with increasing annealing temperature up to 1073 K. The luminescence is very bright to be seen with naked eyes for the sample annealed at 1073 K. From the inset, plot of the I_G/I_R branching ratio vs. anneal temperature, it is obvious that the I_G/I_R branching ratio decrease as the increasing annealing temperature.

The dependence of the green and red up-conversion emission for the sample under 980 nm excitation on temperature is shown in Fig. 7. It can be seen the green and red emission increases significantly with a decreasing sample temperature from 467 to 78 K. This may be explained by increasing ground state population and decreased population of higher levels of the $^4I_{15/2}$ manifold. At 78 K, the green and red up-conversion emission intensities are about 25 and 100 times greater than those at 467 K, respectively. But the emission from $^2H_{11/2}\rightarrow{}^4I_{15/2}$ and $^4S_{3/2}\rightarrow{}^4I_{15/2}$ transition was not observed at 467 K, whereas that of the $^4F_{9/2}\rightarrow{}^4I_{15/2}$ transitions was observed clearly. This result is different from the up-conversion emission of Er^{3+} in other matrixes obtained by our group [15]. In Sun's reports transition to ground state originating from $^2H_{11/2}$ level was not observed as the temperature decreasing to 77 K in YVO_4 nanocrystals.

To study the mechanisms, the up-conversion luminescence intensities of green ($^2H_{11/2}$, $^4S_{3/2}\rightarrow{}^4I_{15/2}$) and red ($^4F_{9/2}\rightarrow{}^4I_{15/2}$) emission have been measured as a function of the pump power. As is well known, the up-conversion emission intensity, I_{up}, is proportional to the nth power of the excitation intensity, I_{IR},

$$I_{up}\propto I_{IR}^{n}$$

where n is the number of IR photons required to convert a visible photon, of which the value is obtained from the slope of the graph of $\ln(I_{up})$ vs. $\ln(I_{IR})$. For the green and

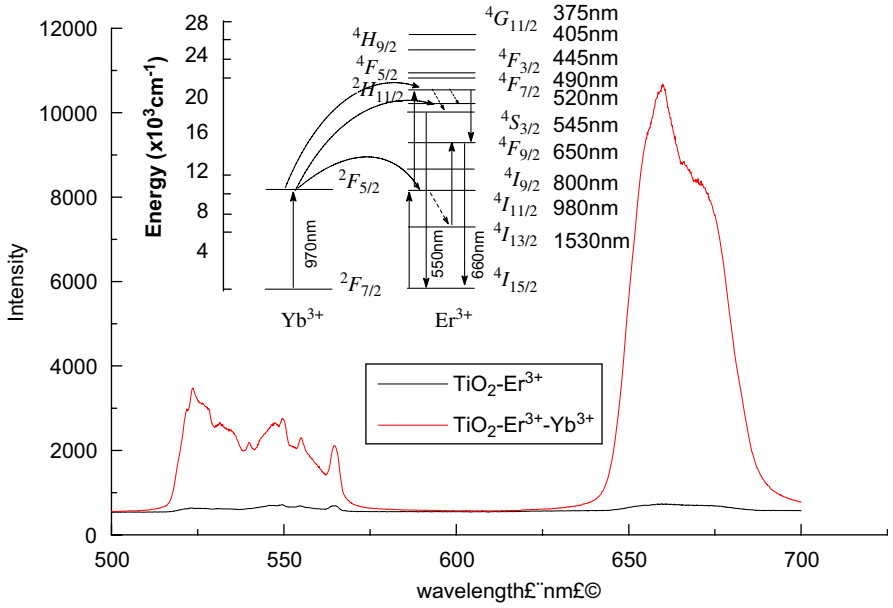

Fig. 5. Up-conversion emission spectra of Er^{3+}–Yb^{3+} co-doped and Er^{3+} doped TiO_2 nanocrystals following excitation with 980 nm when watts is in 527 mW. Inset: Schematic representation of the excited-state adsorption (ESA) and energy-transfer upconversion (ETU) mechanism.

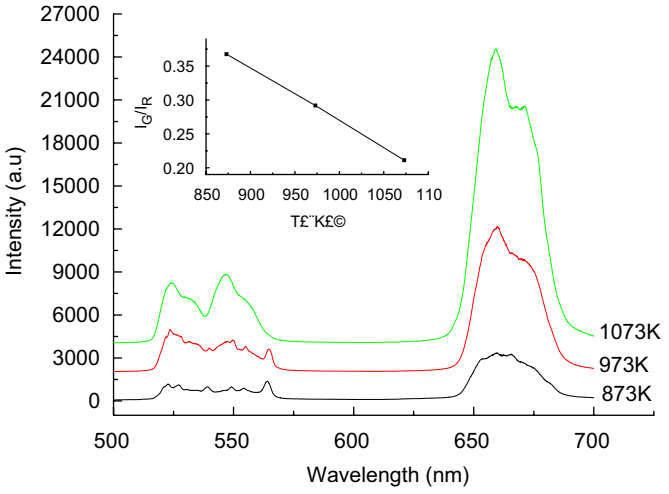

Fig. 6. Up-conversion emission spectra excitation with 980 nm when Watts in is 527 mW of Er^{3+} (10 mol%)–Yb^{3+} (10 mol%) co-doped TiO_2 nanocrystals annealed at different temperature. Inset: Plot of the I_G/I_R branching ratio vs. anneal temperature (G: 525nm, R: 660nm).

red emission in all samples, the plots are shown in Fig. 8, giving a straight line with a slope of 1.97 and 1.52, respectively. Though the slop of 1.52 is not very close to 2, which may be the result of saturation or ground state depletion effect under strong pump power, it still can be concluded that two IR excitation photons are absorbed to produce a visible photon. A two-photon process was thus involved in the up-conversion mechanism responsible for the green and red emission in the Er^{3+}–Yb^{3+} co-doped TiO_2 nanocrystals.

Usually, the up-conversion emission of Er^{3+} can be explained by several well-known mechanisms such as excited-state absorption (ESA), energy transfer up-conversion (ETU). As mentioned above, the dominant up-conversion mechanisms in Er^{3+}–Yb^{3+} co-doped TiO_2 nanocrystals are ESA, which is well explained by our group [15,16], and ETU. The ETU involves not only two closely neighboring Er^{3+} but also Er^{3+} and Yb^{3+}. When Yb^{3+} at $^4F_{5/2}$ state returns nonradiatively to the $^4F_{7/2}$ ground state, its energy is transferred to neighboring Er^{3+} in the $^4I_{11/2}$ state, and then this already excited Er^{3+} ion is excited to the $^4F_{7/2}$ ($^2H_{11/2}$) state through the following channels: $^4I_{11/2} \rightarrow {}^4F_{7/2}$ and $^4I_{13/2} \rightarrow {}^4F_{9/2}$. This is the main pathway by which Yb^{3+} sensitizes the up-conversion process. Transition from $^4S_{3/2}$, $^2H_{11/2}$ excited state to the $^4I_{15/2}$ ground state results in the green emission in 520–570 nm. The 640–690 nm red emission is assigned to the transition from $^4F_{9/2}$ excited state to the $^4I_{15/2}$ ground state. The excited Er^{3+} at $^4I_{13/2}$ level may be populated after different excitation-energy transition and relaxation because of the large Er^{3+} and Yb^{3+} concentration in our samples. Therefore, the most relevant pathway for up-conversion emission initiates with the transition $^4I_{15/2} \rightarrow {}^4I_{13/2}$. Afterwards, excited Er^{3+} ions at $^4I_{13/2}$ level will take one ion to the $^4I_{9/2}$ level. This step is followed by other successive transfer processes from ions at the $^4I_{13/2}$ state, which results in the excitation to higher levels. After nonradiative decay to lower states, radiative transitions to the ground state give rise to the observed red upconverted fluorescence [2].

4. Conclusions

Powders of Er^{3+}–Yb^{3+} co-doped TiO_2 nanocrystals were prepared using sol–gel method. Doping with rare-earth ions affects the phase structure and particle size of TiO_2 nanocrystals. The rutile phase also can be turned to

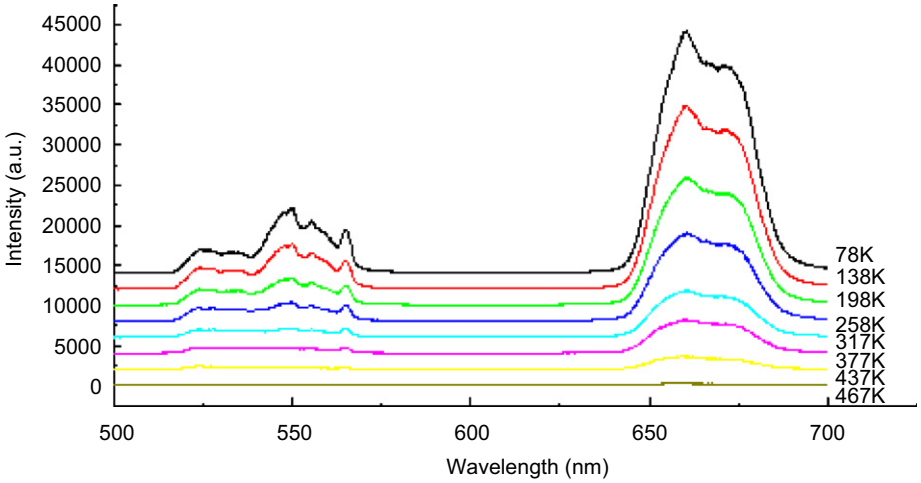

Fig. 7. The up-conversion fluorescence emission spectra of Er^{3+} (10 mol%)–Yb^{3+} (10 mol%) co-doped TiO_2 nanocrystals at different measured temperature (excitation with 980 nm, watts is in 527 mW).

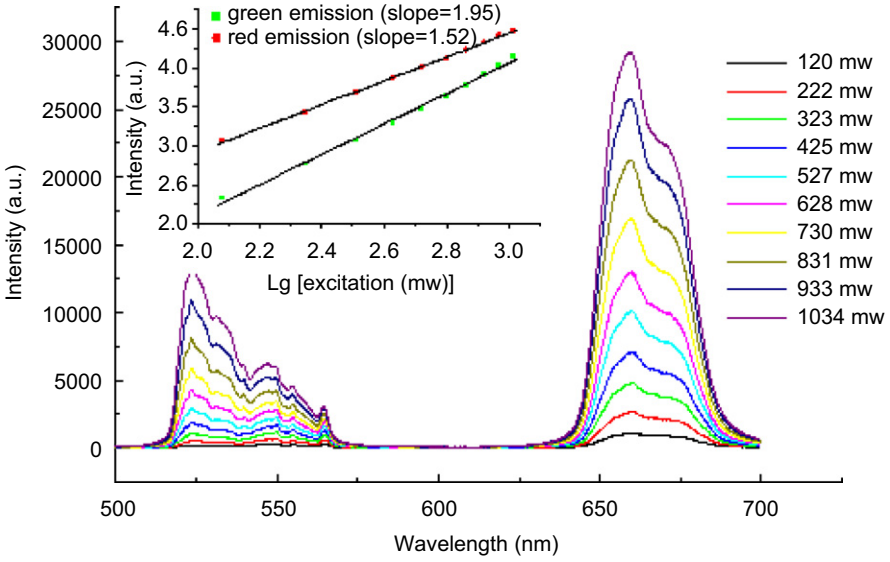

Fig. 8. Power dependence of the up-conversion luminescence in Er^{3+} (10 mol%)–Yb^{3+} (10 mol%) co-doped TiO_2 nanocrystals excited at 980 nm. Inset: Graph of $\log(I_{UC})$ vs. $\log(I_{Pump})$ for the sample.

anatase phase with increasing calcinations temperature. Upon UV excitation of the TiO_2 matrix, the energy transfer to the Er^{3+} ions occurs and the characteristic luminescence of the f–f transition is observed. The green (520–570 nm) and red (640–690 nm) up-conversion emission in Er^{3+} doped and Er^{3+}–Yb^{3+} co-doped TiO_2 nanocrystals powders were obtained, They were associated with ($^2H_{11/2}$, $^4S_{3/2}\rightarrow{}^4I_{15/2}$) and ($^4F_{9/2}\rightarrow{}^4I_{15/2}$) transfer of Er^{3+}, respectively. Both of the green and red up-conversion emission intensities were proved to increase with increasing calcinations temperature from 873 to 1073 K and decreasing measure temperature from 467 to 78 K. The up-conversion process is most efficient for the large particles as well as other reports [17,18]. According to the energy level diagram of Er^{3+} and Yb^{3+} ion and the relationship between I_{up} and I_{IR}, the up-converted emission mechanism for Er^{3+}–Yb^{3+} co-doped TiO_2 nanocrystals sample is confirmed as ESA and ETU under 980 nm infrared excitation.

Acknowledgments

The authors gratefully acknowledge the financial support of the National Nature Science Foundation of China (Grant no. 10674132 and 60601015) and Science and Technology Development Foundation of Jilin Province (no. 20060572).

References

[1] A.J. Silversmith, W. Lenth, R.M. Macfarlane, Appl. Phys. Lett. 51 (1987) 1977.

[2] G.S. Maciel, C.B. De Araujo, Y. Messaddeq, M.A. Aegerter, Phys. Rev. B 55 (1997) 6335.
[3] R. Kappor, C.S. Friend, A. Biswas, P.N. Prasad, Opt. Lett. 25 (2000) 338.
[4] M. Pollnau, D.R. Gamelin, S.R. Luthi, H.U. Gudel, M.P. Hehelen, Phys. Rev. B 61 (2001) 3337.
[5] P.S. Golding, S.D. Jackson, T.A. King, M. Pollnau, Phys. Rev. B 62 (2000) 856.
[6] J. Silver, M.I. Martinez-Rubio, T.G. Ireland, G.R. Fern, R. Withnall, J. Phys. Chem. B 105 (2001) 948.
[7] G.C. Yi, B.A. Block, G.M. Ford, B.W. Wessels, Appl. Phys. Lett. 73 (1998) 1625.
[8] H.X. Zhang, C.H. Kam, Y. Hou, X.Q. Han, S. Buddhudu, Q. Xiang, Y.L. Lam, Y.C. Chan, Appl. Phys. Lett. 77 (2000) 609.
[9] S. Sivakumar, F.C. van Veggel, M. Raudsepp, J. Am. Chem. Soc. 127 (2005) 12464.
[10] G.S. Yi, H.C. Lu, S.Y. Zhao, Y. Ge, W.J. Yang, D.P. Chen, L.H. Guo, Nano Lett. 4 (2004) 2191.
[11] S.-Y. Chen, C.-C. Ting, W.-F. Hsieh, Thin Solid Film 434 (2003) 171.
[12] H. Nii, K. Ozaki, M. Herren, M. Morita, J. Lumin. 116 (1998) 76.
[13] E. Snoeks, G.N. vanden Hoven, A. Polman, B. Hendriksen, M.B.J. Diemeer, F. Priolo, J. Opt. Soc. Am. B 12 (1997) 1468.
[14] Ulrike Diebold Surface Science Reports. 48 (2003) 53–229.
[15] Y. Sun, H. Liu, X. Wang, X. Kong, H. Zhang, Chem. Mater. 18 (2006) 2726.
[16] X. Wang, X. Kong, G. Shan, Y. Yu, Y. Sun, L. Feng, K. Chao, S.Z. Lu, Y. Li, J. Phys. Chem. B 108 (2004) 18408.
[17] A. Patra, Christopher S. Friend, R. Kapoor, Paras N. Prasad, Chem. Mater. 15 (2003) 3650–3655.
[18] J. Silver, M.I. Martinez-Rubio, T.G. Ireland, G.R. Fern, R. Withnall, J. Phys. Chem. 105 (2001) 948.